

Simple low-dimensional computations explain variability in neuronal activity

Christopher W. Lynn^{1,2,3}

¹*Department of Physics, Yale University, New Haven, CT 06520, USA*

²*Quantitative Biology Institute, Yale University, New Haven, CT 06520, USA*

³*Wu Tsai Institute, Yale University, New Haven, CT 06520, USA*

Abstract

Our understanding of neural computation is founded on the assumption that neurons fire in response to a linear summation of inputs.^{1–4} Yet experiments demonstrate that some neurons are capable of complex computations that require interactions between inputs.^{5–9} Here we show, across multiple brain regions and species,^{10–12} that simple computations (without interactions between inputs) explain most of the variability in neuronal activity. Neurons are quantitatively described by models that capture the measured dependence on each input individually, but assume nothing about combinations of inputs. These minimal models, which are equivalent to binary artificial neurons, predict complex higher-order dependencies and recover known features of synaptic connectivity.^{13–15} The inferred computations are low-dimensional, indicating a highly redundant neural code that is necessary for error correction. These results suggest that, despite intricate biophysical details, most neurons perform simple computations typically reserved for artificial models.

Main

Neurons receive synaptic inputs from tens of other neurons in the roundworm *C. elegans*,¹³ hundreds to thousands in the fruit fly,¹⁵ and thousands to tens of thousands in mice, monkeys, and humans.¹⁴ As the number of inputs grows, the space of possible computations explodes exponentially. To tame this complexity, simplified models have long assumed that the output of a neuron can be described as a linear sum of inputs followed by a nonlinear threshold.^{1–4, 16, 17} While this picture forms the foundation for our understanding of neural computation, both in the brain and artificial networks, it has not been systematically tested.

Across different species and neural systems, it is now possible to make long, stable recordings of large contiguous populations of neurons.^{10–12, 18, 19} This means that for each neuron, we may have access to its output and all of its inputs simultaneously. But how can we determine whether the activity of each neuron arises from a simple computation, or instead, requires complex interactions between inputs? To answer this question, we need a framework to quantify the minimal consequences of simple computations.

Minimal computations

Neurons in the brain receive inputs at their dendrites and then execute a binary function: they either remain silent ($y = 0$) or generate a discrete impulse ($y = 1$) known as an action potential or spike (Fig. 1a).^{20, 21} This mapping from inputs to output involves intricate details of membrane potential dynamics and cell morphology, which vary between neurons, brain regions, and species.^{22–24} Yet for every neuron, these details culminate in a table of firing probabilities $P(y = 1|x_1, \dots, x_n)$, which define the computation that the cell performs on its n inputs x_1, \dots, x_n . This description, while general enough to capture every neuron, is also hopelessly complex; it requires specifying a different firing probability for each combination of inputs, a number that grows exponentially with n (Fig. 1b). To understand neuronal computations, we thus need simplifying hypotheses.

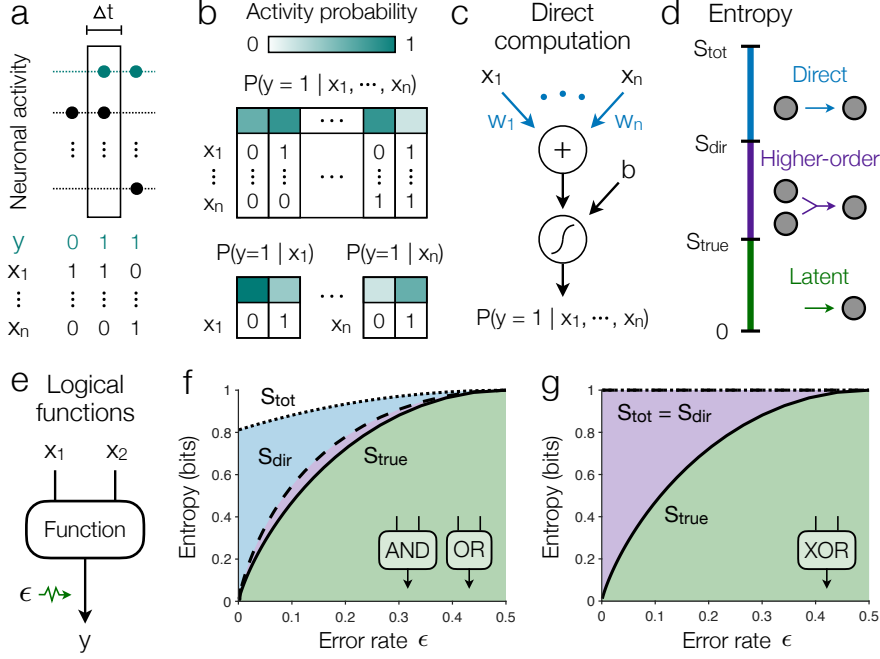


Fig. 1 | Minimal model of direct computations. **a**, Spiking activity (dots) of an output neuron y and n inputs x_1, \dots, x_n . Within a window of width Δt , each neuron binarizes into active ($y = 1$) or silent ($y = 0$).^{20,21} **b**, The computation performed by the output is defined by the probability of firing in response to each of the 2^n combinations of inputs (*top*). The simplest dependencies—those between the output and each input individually—are defined by direct firing probabilities, the number of which grows linearly with n (*bottom*). **c**, The minimal computation, which has maximum entropy consistent with these direct dependencies,^{25,26} is equivalent to a logistic artificial neuron.⁴ **d**, Hierarchy of entropies, where the difference $S_{\text{tot}} - S_{\text{dir}}$ quantifies the amount of variability captured by direct dependencies, $S_{\text{dir}} - S_{\text{true}}$ the variability due to higher-order dependencies, and S_{true} the inherent variability due to latent variables.²⁷ **e**, Computation defined by a logical function with error probability ϵ and binary inputs that are independently drawn at random. **f-g**, Hierarchy of entropies as functions of error rate for the AND and OR functions (**f**) and the XOR function (**g**). For AND and OR (**f**), the computation is almost exactly captured by direct dependencies ($S_{\text{dir}} \approx S_{\text{true}}$), while for XOR (**g**), these simple dependencies provide no information about the output ($S_{\text{dir}} = S_{\text{tot}}$).

The simplest relationships between the output y and inputs x_i are contained in the direct dependencies $P(y|x_i)$; these capture everything about the computation that does not involve interactions between inputs. But how can we tell whether these simple dependencies are enough to describe a real neuron? Even if we measure all the direct dependencies $P(y|x_1), \dots, P(y|x_n)$, there are still an infinite number of possible computations $P(y|x_1, \dots, x_n)$ consistent with these constraints. Our problem, therefore, is to find the computation that matches these simple depen-

dencies, but is maximally random with regard to higher-order dependencies involving two, three, or more inputs. We show that this minimal computation, which has maximum entropy consistent with the direct dependencies,^{25,26} takes the form

$$P(y = 1|x_1, \dots, x_n) = \sigma\left(b + \sum_{i=1}^n w_i x_i\right), \quad (1)$$

where $\sigma(\cdot)$ is the logistic function (Methods). The parameters b and w_i must be computed so that the model matches the measured direct dependencies, and we provide an algorithm that converges efficiently, even for large n (Methods).

This theory, our first main result, establishes a concrete connection between biological and artificial neurons: A real neuron with purely direct dependencies is equivalent to an artificial neuron with bias b , linear weights w_i , and logistic activation function (Fig. 1c).⁴ Consequently, all other artificial neurons—for example, with rectified or piecewise linear activations—must implicitly assume higher-order dependencies and therefore interactions between their inputs.^{28,29}

We are now prepared to study the amount of variability captured by direct dependencies. The total variability of a neuron is quantified by the entropy S_{tot} of its output with no knowledge of the inputs.³⁰ By contrast, the true entropy of a neuron S_{true} quantifies the latent variability in its computation that cannot be explained by the inputs (Methods).²⁶ With knowledge of only the direct dependencies, the entropy S_{dir} of the minimal model in Eq. (1) sits between these two extremes (Methods), yielding a hierarchy $S_{\text{tot}} \geq S_{\text{dir}} \geq S_{\text{true}} \geq 0$. In this way, the difference $S_{\text{tot}} - S_{\text{dir}}$ defines the amount of variability captured by direct dependencies, while the remaining variability S_{dir} can only arise from higher-order dependencies or latent variables (Fig. 1d).²⁷ Importantly, if the direct entropy S_{dir} becomes small, then so too does the true entropy S_{true} . In this limit, the model (and thus the neuron itself) becomes equivalent to a McCulloch-Pitts (MP) neuron,¹ or a perceptron,³¹ and all the variability is explained by direct dependencies.

To gain intuition, consider an output y that performs a logical function on two binary inputs x_1 and x_2 with error rate ϵ (Fig. 1e). For AND and OR gates, as ϵ increases, the output becomes more stochastic, leading to higher variability (Fig. 1f). Across all error rates ϵ , we find that the

direct entropy S_{dir} lies close to the true entropy S_{true} , such that the model provides a tight approximation to the true computation. As errors vanish and the output becomes deterministic ($\epsilon = 0$), the minimal model becomes exact ($S_{\text{dir}} = S_{\text{true}}$) and all the variability in y is explained by direct dependencies ($S_{\text{dir}} = 0$). This reflects the fact that AND and OR are linearly separable functions and thus are exactly described by a perceptron, which (as discussed above) is a purely direct computation.³² For comparison, consider the XOR function, the classic example of a higher-order computation that depends irreducibly on the specific combination of inputs x_1 and x_2 (Fig. 1g). We find that direct dependencies provide no information about the computation ($S_{\text{dir}} = S_{\text{tot}}$), such that all the variability arises from either higher-order dependencies or latent stochasticity. Together, these results demonstrate how, even in simple cases, computations can be decomposed into their constituent parts.

Identifying optimal inputs

To study the computation of a real neuron, we must first specify its inputs. In large-scale recordings, while synaptic connectivity is rarely known, we can infer the optimal inputs that provide the best description of a neuron’s output. In a population of N neurons, for a given output neuron, we would like to select the $n < N$ inputs that, once included in the minimal computation [Eq. (1)], reduce our uncertainty about the output S_{dir} as much as possible (Methods). This minimax entropy problem is generally intractable;^{33,34} however, we provide an efficient algorithm that greedily identifies the locally optimal inputs at each step (Methods). The result is a set of n inputs that, by minimizing the model uncertainty S_{dir} , also maximize the amount of variability captured by direct dependencies $S_{\text{tot}} - S_{\text{dir}}$.

Consider a large population of neurons in the mouse hippocampus (Methods).¹¹ These cells play key roles in encoding the animal’s location, mapping features in its environment, and storing memories of past events;^{35–38} yet it remains unclear whether these functions arise from simple computations. For a given output neuron, we can infer the optimal n inputs and the corresponding minimal computation (Fig. 2a). We only consider inputs that co-activate with the output at least

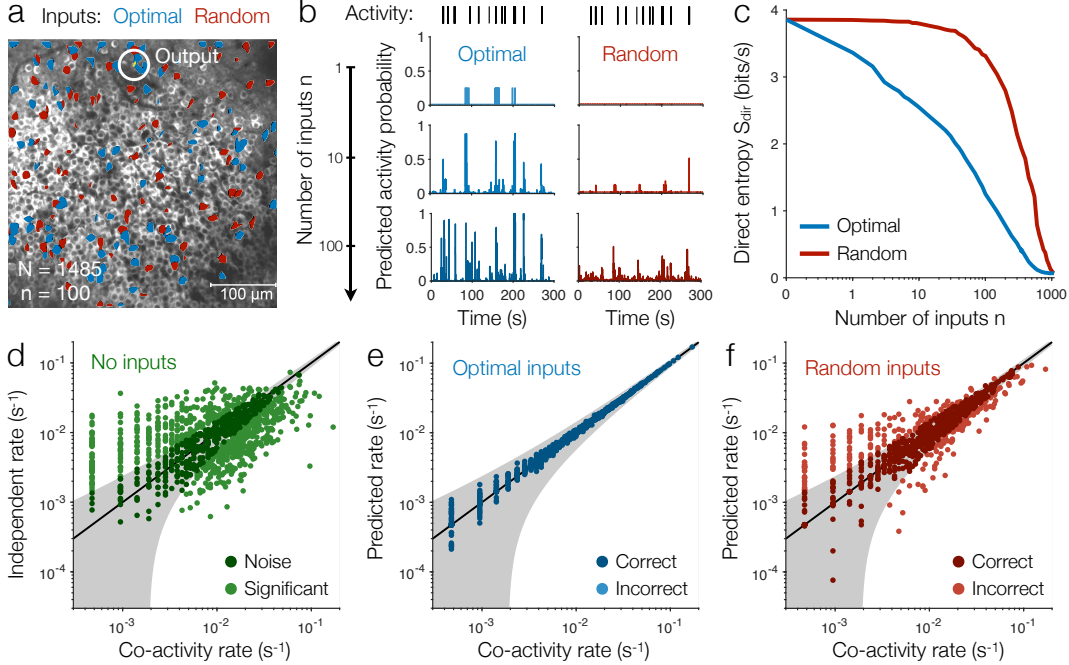


Fig. 2 | Identifying a minimal set of optimal inputs. **a**, Population of $N = 1485$ neurons in the mouse hippocampus recorded as the animal runs along a virtual track (Methods).^{11,35} For a randomly-selected output neuron (circle), we illustrate the $n = 100$ optimal input neurons (blue) and an equal number of random inputs (red). **b**, True output activity (top) and activity probabilities predicted by the minimal model [Eq. (1)] for increasing numbers of optimal inputs (left) and random inputs (right) within a five-minute window. **c**, Entropy of the minimal direct computation S_{dir} versus the number of inputs n for optimal inputs (blue) and random inputs (red). **d**, Co-activity rates between the output and all other neurons versus those predicted by the independent model with no inputs; line indicates equality, and shaded region indicates experimental errors (two standard deviations). **e**, With $n^* = 350$ optimal inputs, the minimal model correctly predicts all remaining co-activity rates, and thus all direct dependencies on other neurons in the population (Methods). **f**, With the same number of random inputs, the minimal computation fails to predict many co-activity rates.

once, which guarantees that the direct dependencies are well-defined (Methods). As the number of inputs increases, the minimal direct model quickly becomes expressive, making increasingly accurate predictions for the output activity (Fig. 2b). In fact, despite being maximally random with respect to higher-order dependencies, the entropy of the direct computation S_{dir} drops exponentially with the number of inputs (Fig. 2c). This means that with only a relatively small number of inputs, direct dependencies capture an exponentially large amount of variability $S_{\text{tot}} - S_{\text{dir}}$.

By contrast, with random inputs, the direct computation fails dramatically, explaining effectively none of the variability until almost all the inputs are included (Fig. 2c). This suggests that by including all possible inputs, we risk overfitting the output, thus leading to an artificially low entropy S_{dir} . To avoid overfitting, we introduce the following regularization: We select the minimal number of inputs n^* needed to predict all other direct dependencies in the population (Methods). This ensures that we do not fit any input-output dependencies that the model already predicts (Supplementary Information). The result is a combined framework for inferring the minimal computation [Eq. (1)] with the minimal set of inputs.

For the neuron in Fig. 2, among its positive correlations with other neurons, 66% are significant, meaning that 34% can be predicted with no inputs at all (Fig. 2d). We identify a minimal set of $n^* = 350$ inputs that are sufficient to predict all of the direct dependencies (Fig. 2e); these minimal inputs explain $(S_{\text{tot}} - S_{\text{dir}})/S_{\text{tot}} = 89\%$ of the output's variability. For comparison, with the same number of randomly-selected inputs, many of the output's correlations remain unexplained (Fig. 2f). These findings establish that the vast majority of neuronal variability, at least for one cell, is captured by a purely direct computation with a relatively small number of inputs.

Minimal computations across systems and species

We can repeat this calculation for many neurons spanning different brain regions and species. Across the $N = 1485$ neurons in the hippocampus (Fig. 2a),^{11,35} we confirm that the direct entropy S_{dir} drops exponentially with the number of inputs (Fig. 3a). This decrease is so sharp that, for the median neuron, the first input explains 17% of the variability, and only 15 inputs are needed to explain 50% of the variability. With $n^* = 214$ inputs, the minimal computation captures all of a neuron's direct dependencies. These models, which we refer to as complete, explain over 90% of a neuron's entropy S_{tot} , leaving less than 10% for higher-order dependencies and inherent stochasticity.

In an even larger population of $N > 10^4$ cells in the mouse visual cortex,¹⁰ for each neuron,

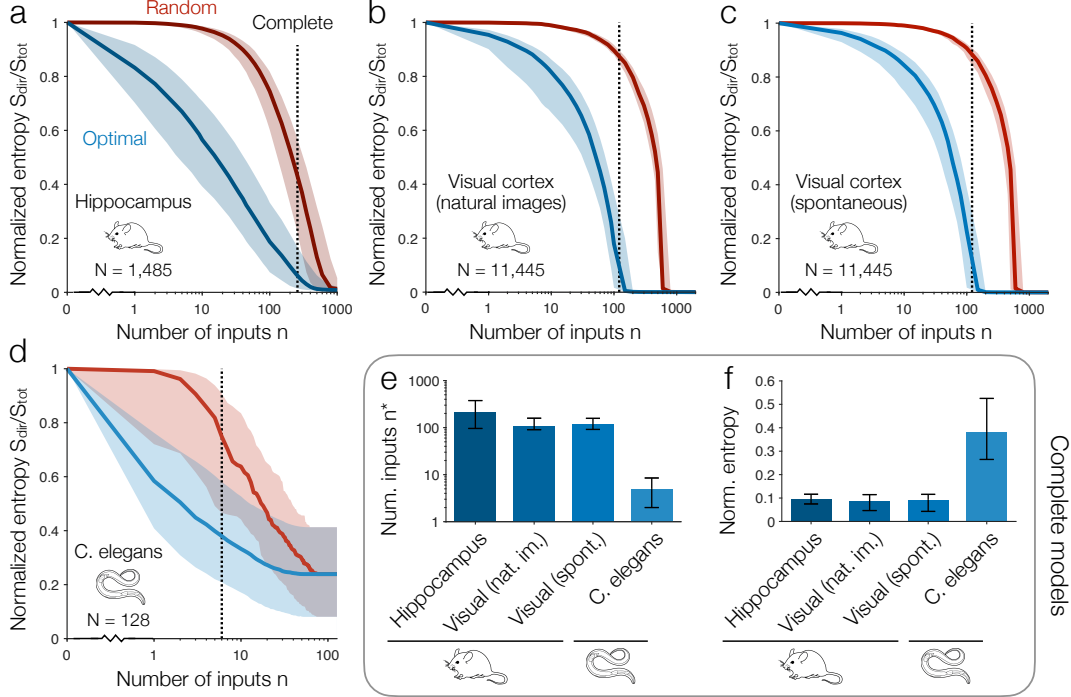


Fig. 3 | Simple low-dimensional computations across systems and species. **a**, Entropy of the minimal computation S_{dir} normalized by total entropy S_{tot} for n inputs chosen optimally (blue) or randomly (red). Lines and shaded regions represent medians and interquartile ranges across all $N = 1485$ of the hippocampal neurons in Fig. 2.^{11,35} Dashed line indicates the minimal number of inputs n^* needed to capture all the direct dependencies for the median neuron. **b-d**, Normalized model entropy $S_{\text{dir}}/S_{\text{tot}}$ versus number of inputs n for 100 random output neurons within a population of $N = 11,445$ cells in the mouse visual cortex during responses to natural images (**b**) and spontaneous activity (**c**)¹⁰ and for $N = 128$ neurons in the brain of *C. elegans* (**d**).¹² See Methods for experimental details. **e-f**, For the complete minimal computations in **a-d**, we compare the minimal number of inputs n^* needed to capture all direct dependencies (**e**) and the normalized entropies $S_{\text{dir}}/S_{\text{tot}}$ (**f**). Values and error bars represent medians and interquartile ranges across neurons.

one might expect that more inputs are needed to capture all the direct dependencies. However, when responding to natural images, the median neuron only requires $n^* = 108$ inputs (less than 1% of the entire population) to predict the remaining 99% of its direct dependencies (Fig. 3b). Moreover, just as in the hippocampus, these complete computations explain 91% of each neuron's variability. For spontaneous activity in the same population, we observe nearly identical results (Fig. 3c). Thus, across the hippocampus and visual cortex, neurons are consistently described by

computations that are purely direct and nearly deterministic; that is, by perceptrons.

Finally, in the roundworm *C. elegans*, one can record from the entire brain, such that for each cell, we have access to nearly all its inputs.¹² For the median neuron, a minimal set of $n^* = 5$ inputs is sufficient to predict all other direct dependencies in the brain. These remarkably simple computations explain 62% of each neuron's variability S_{tot} (Fig. 3d). Together, these findings (summarized in Fig. 3e-f) comprise our second main result: That neuronal activity, spanning multiple systems and species, appears to arise from computations that are simple (involving only direct dependencies) and low-dimensional (with a relatively small number of inputs).

Predicting higher-order dependencies

While complex computations require networks of artificial neurons,^{4,31,32} in real neurons, interactions between dendrites can lead to higher-order dependencies that are responsible for gating and even linearly non-separable functions like XOR (Fig. 1g).⁵⁻⁹ However, the accuracy of our minimal model suggests that, with knowledge of only the direct dependencies on individual inputs, we should be able to predict the higher-order dependencies on combinations of inputs. If true, this would paint a surprisingly simple picture in which higher-order dependencies arise naturally from direct dependencies.

To explain the k^{th} -order dependence $P(y|x_1, \dots, x_k)$, it is sufficient to predict the correlations between the output y and all subsets of the k inputs (Methods). For 2nd-order dependencies $P(y|x_i, x_j)$, because our minimal computation captures all of the direct dependencies (either by fitting or by prediction), all that remain are the 2nd-order correlations between the output y and pairs of neurons x_i and x_j . In the hippocampus, our minimal model predicts 99.85% of these correlations (within experimental errors), leaving only 0.15% of the 2nd-order dependencies unexplained by simpler direct dependencies (Fig. 7a). For comparison, with the same number of random inputs, the minimal model fails to predict many of the 2nd-order dependencies (Fig. 7b). With optimal inputs, the accuracy of the minimal computation increases as we study dependencies

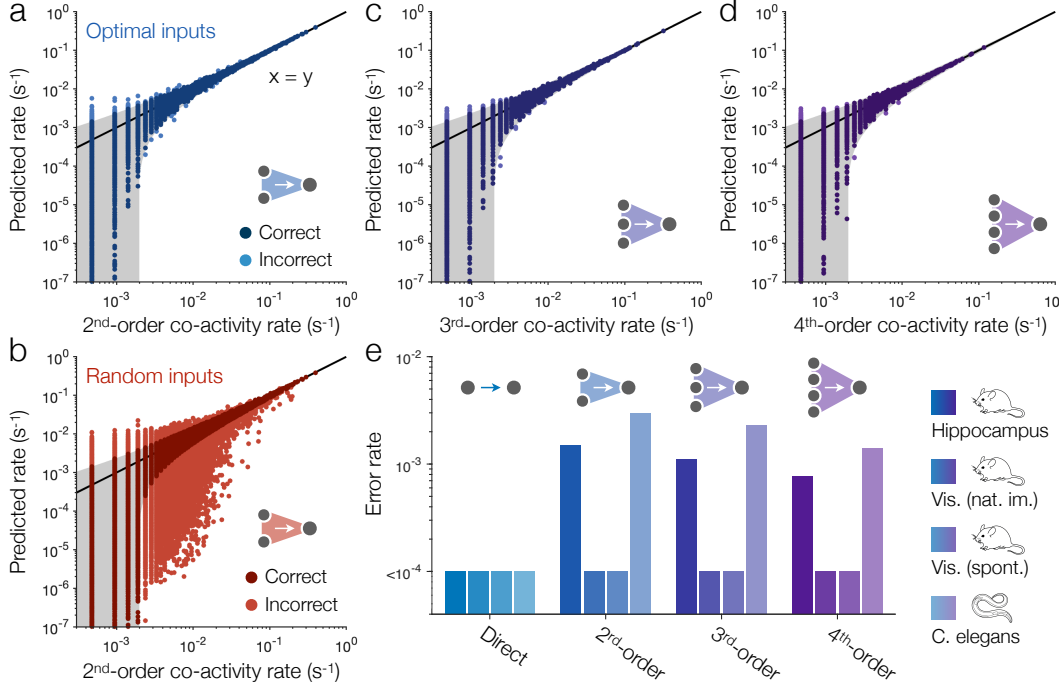


Fig. 7 | Predicting higher-order dependencies. **a**, For the hippocampal population (Fig. 2),^{11,35} we plot the 2nd-order co-activity rates predicted by the complete minimal models versus those measured in data. Line indicates equality, shaded region indicates experimental errors (two standard deviations), dark points are correct (within errors), and light points are incorrect. **b**, 2nd-order co-activity rates predicted by minimal computations with random inputs. **c-d**, 3rd-order (**c**) and 4th-order (**d**) co-activity rates predicted by minimal models with optimal inputs. In **a-d**, for each output neuron we consider 100 randomly-selected pairs (**a-b**), triplets (**c**), and quadruplets (**d**) of input neurons. **e**, Fractions of co-activity rates that are not explained by direct dependencies for populations in the mouse hippocampus,¹¹ the mouse visual cortex during responses to natural images and spontaneous activity,¹⁰ and the brain of *C. elegans*¹² (Supplementary Information).

of even higher order. Minimal computations fail to predict only 0.11% of the 3rd-order correlations (Fig. 7c), and this fraction drops to 0.08% for 4th-order correlations (Fig. 7d). These results in the mouse hippocampus are recapitulated in the mouse cortex and *C. elegans* (Fig. 7e). We therefore find, consistently across many neurons, that the vast majority of higher-order dependencies arise from simpler direct dependencies, rather relying on interactions between inputs.

Inferred computations and error correction

As previously derived, the maximum entropy computation consistent with direct dependencies is equivalent to a logistic artificial neuron with bias b and weights w_i [Eq. (1)]. In the hippocampal population, all cells have negative biases, leading them to favor silence over activity (Fig. 6a). Meanwhile, the weights, which produce correlations between neurons (Fig. 6b), exhibit four key features. First, as discussed above, the weights are sparse, with only a small number of inputs n^* needed to explain all of a neuron's direct dependencies (Fig. 3e). Second, the distribution of magnitudes is heavy-tailed (specifically log-normal), with some rare weights that are orders of magnitude stronger than average (Fig. 6c). Third, the weights are evenly split between positive and negative, reflecting a delicate balance between excitatory and inhibitory interactions (Fig. 6c). Finally, unlike existing maximum entropy models,^{21,33,35} the weights are highly directed, with the connection strength from input i to output j differing significantly from the reverse. These sparse, heavy-tailed, balanced, and directed weights are universal features of synaptic connectivity observed across brain regions and species.^{14,15,39–42}

The connections from the inputs to the output enable the flow of information; for each neuron, this mutual information is the drop in entropy $I_{\text{true}} = S_{\text{tot}} - S_{\text{true}}$.^{26,30} While this is impossible to estimate directly, our minimal computation provides a tractable lower bound, equal to the amount of variability explained by direct dependencies $I_{\text{dir}} = S_{\text{tot}} - S_{\text{dir}}$ (Methods). Moreover, since direct dependencies capture nearly all of the variability in activity (Fig. 3f), we know that this lower bound is tight, with $0.9I_{\text{true}} \lesssim I_{\text{dir}} \leq I_{\text{true}}$ for the mouse hippocampus and visual cortex. Across neurons, we find that this direct information increases linearly with the number of inputs n^* , with each input communicating 0.01 bits/s to the output on average (Fig. 6d). By symmetry, I_{dir} also defines the amount of information that each neuron encodes about the rest of the population. For each bit generated by a neuron, we find that a consistent 0.87 encode information about its inputs (Fig. 6e). This large proportion of information concentrated on a small number of inputs indicates a highly redundant neural code. As in a Hopfield network, specifying the states of a small number of cells should be sufficient to predict the rest, thus yielding error correction.^{2,17,21}

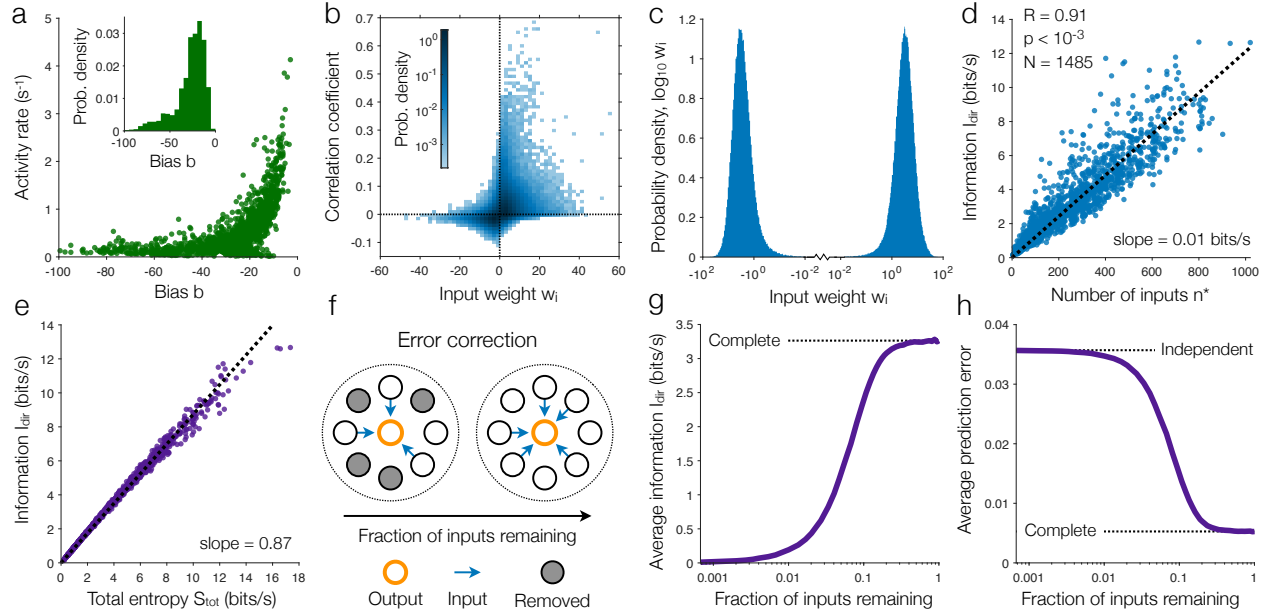


Fig. 6 | Realistic connectivity and robust computations. **a**, Firing rate versus inferred bias b for each neuron in the hippocampal population, and distribution of inferred biases (inset).¹¹ **b**, Probability density of the correlation coefficient and corresponding input weight w_i over all input-output pairs. **c**, Distribution of inferred input weights w_i over all input-output pairs in the population. **d**, Information I_{dir} versus number of inputs n^* across all neurons; dashed line indicates linear fit. **e**, Input-output information I_{dir} versus total entropy S_{tot} across all neurons; dashed line indicates linear fit. **f**, Illustration of error correction analysis. We remove neurons from the population by marginalizing over their states and study the predicted computations for the remaining neurons (Methods). **g**, Input-output information I_{dir} as a function of the fraction of inputs remaining for each neuron; dashed line illustrates the value for the full model with all inputs. **h**, Prediction error for the minimal direct model with different fractions of the inputs removed; dashed lines indicate the values for the full model with all inputs (bottom) and the independent model with no inputs (top). In panels **g** and **h**, values are averaged over neurons and 100 repeats of simulated ablations (Methods).

To test this hypothesis, we can artificially remove, or ablate, some of the cells from the population by marginalizing over their states (Methods). For each of the remaining neurons, we can then investigate the impact on its computation (Fig. 6f). As each neuron loses more of its inputs, the flow of information from inputs to output undergoes a sharp transition (Fig. 6g). Above this transition, neurons can lose the vast majority of their inputs without impacting the flow of information, while below the transition, almost no information is communicated. Similarly, we can remove most of the inputs to a neuron before our model fails to accurately predict its activity (Fig. 6h).

These findings demonstrate that the inferred computations are strikingly robust, maintaining nearly the same output activity even after losing the majority of their inputs.

Discussion

Despite intricate morphologies and biophysical dynamics,^{5–9,22–24} neurons have long been studied using models of simple computations.^{1–4,17,31} Here, we develop a framework to study whether neuronal activity arises from the simplest possible computations: those that depend on each input individually, but are maximally random with regard to complex higher-order dependencies. Across the mouse hippocampus and visual cortex,^{10,11,35} these direct dependencies explain 90% of the variability in neuronal activity (Fig. 3), leaving only 10% for interactions between inputs and inherent stochasticity (Fig. 1). Moreover, the inferred models—which are equivalent to artificial neurons—predict the higher-order dependencies on combinations of inputs (Fig. 7), recover salient features of synaptic connectivity (Fig. 6), and are inherently low-dimensional (Fig. 3).

These results immediately raise future questions about the nature of neuronal computations. As experiments advance to record from larger populations across species, neural systems, and imaging modalities,^{10–12,18,19,43} does neuronal activity consistently arise from minimal computations? Additionally, by wiring the models of different neurons together, we arrive at a highly recurrent neural network.^{2,16,17,21,33,35} What can such networks reveal about the computational and dynamical properties of populations as a whole? Finally, because each model is derived from the statistical dependencies between neurons, the inferred connectivity may reflect not only causal interactions, but also functional correlations due to latent variables. If the underlying population is defined by an Ising model—equivalent to a stochastic Hopfield network,² Boltzmann machine,⁴⁴ or maximum entropy model^{21,33–35}—then we show that the inferred computations recover the true underlying interactions (Supplementary Information). As connectomes mapping the wiring between neurons become increasingly available,^{13–15,45,46} how does the inferred connectivity relate to underlying synaptic connectivity? The framework presented here provides the tools to begin answering these questions.

Methods

Minimal computations. Consider a binary output $y \in \{0, 1\}$ and a set of n binary inputs $\mathbf{x} = \{x_1, \dots, x_n\} \in \{0, 1\}^n$. From experiments, we have samples of activity $y(\ell)$ and $\mathbf{x}(\ell)$, where $\ell = 1, \dots, L$. From this data, we can compute the direct dependencies $P(y|x_i)$ for all inputs $i = 1, \dots, n$. We want to derive the computation $P(y|\mathbf{x})$ that is consistent with these direct dependencies and has maximum entropy

$$S(P) = - \left\langle \sum_y P(y|\mathbf{x}) \log P(y|\mathbf{x}) \right\rangle_{\mathbf{x}}, \quad (2)$$

where $\langle f(\mathbf{x}) \rangle_{\mathbf{x}} = \frac{1}{L} \sum_{\ell} f(\mathbf{x}(\ell))$ denotes an empirical average over the inputs, and (unless otherwise specified) we use log base two such that entropy is measured in bits.^{25,26} Each direct dependence $P(y|x_i)$ is uniquely defined by the averages $\langle y \rangle = \frac{1}{L} \sum_{\ell} y(\ell)$, $\langle x_i \rangle = \frac{1}{L} \sum_{\ell} x_i(\ell)$, and $\langle yx_i \rangle = \frac{1}{L} \sum_{\ell} y(\ell)x_i(\ell)$. For all computations $P(y|\mathbf{x})$, we have $\langle x_i \rangle_P = \langle x_i \rangle$, where $\langle f(y, \mathbf{x}) \rangle_P = \langle \sum_y f(y, \mathbf{x}) P(y|\mathbf{x}) \rangle_{\mathbf{x}}$ denotes a model average. Thus, one only needs to constrain the average firing rate $\langle y \rangle$ and the correlations $\langle yx_i \rangle$ for all inputs. The appropriate Lagrangian is therefore

$$L = S(P) + b(\langle y \rangle_P - \langle y \rangle) + \sum_i w_i (\langle yx_i \rangle_P - \langle yx_i \rangle) + \sum_{\mathbf{x}} \lambda(\mathbf{x}) \left(\sum_y P(y|\mathbf{x}) - 1 \right), \quad (3)$$

where the Lagrange multipliers b , w_i , and $\lambda(\mathbf{x})$ constrain $\langle y \rangle_P = \langle y \rangle$, $\langle yx_i \rangle_P = \langle yx_i \rangle$, and the normalization, respectively. Maximizing with respect to $P(y|\mathbf{x})$, we arrive at the minimal direct computation

$$P(y|\mathbf{x}) = \frac{1}{Z(\mathbf{x})} e^{y(b + \sum_i w_i x_i)}, \quad (4)$$

where $Z(\mathbf{x}) = 1 + e^{b + \sum_i w_i x_i}$ ensures normalization. The activity probability is thus given by $P(y=1|\mathbf{x}) = \sigma(b + \sum_i w_i x_i)$, where $\sigma(\cdot)$ is the logistic function. Mathematically, this minimal computation is closely related to generalized linear models,⁴⁷ which have provided key insights into neural dynamics.⁴⁸

Computing model parameters. Even with the functional form for the minimal computation, the model is still not complete. The bias b and weights w_i must be computed so that the model matches the measured average $\langle y \rangle$ and correlations $\langle yx_i \rangle$ for all inputs i . Letting $Q(y|\mathbf{x})$ denote the true computation, the Kullback-Leibler (KL) divergence with the model is

$$D_{\text{KL}}(Q||P) = \left\langle \sum_y Q(y|\mathbf{x}) \ln \frac{Q(y|\mathbf{x})}{P(y|\mathbf{x})} \right\rangle_{\mathbf{x}}. \quad (5)$$

To fit the model parameters, we perform gradient descent in the KL divergence, with gradients given by $\nabla_b D_{\text{KL}}(Q||P) = \langle y \rangle_P - \langle y \rangle$ and $\nabla_{w_i} D_{\text{KL}}(Q||P) = \langle yx_i \rangle_P - \langle yx_i \rangle$. Unlike traditional maximum entropy models, which require costly Monte Carlo simulations,^{21,35,49} the above gradients simply involve empirical averages $\langle \cdot \rangle_{\mathbf{x}}$. This means that gradient descent converges efficiently, even for very large n .

Information in direct dependencies. The entropy of the true computation $S_{\text{true}} = S(Q)$ defines the latent variability that cannot be explained by input-output dependencies of any order; however, unless the number of inputs n is small,

S_{true} cannot be estimated directly. The total variability of the neuron with no knowledge of the inputs is defined by the entropy S_{tot} of the marginal $P(y)$.³⁰ Between these two extremes, with knowledge of only the direct dependencies $P(y|x_i)$, the entropy (in nats) of the minimal computation [Eq. (8)] is given by

$$S_{\text{dir}} = \langle \log Z(\mathbf{x}) \rangle_{\mathbf{x}} - b\langle y \rangle - \sum_i w_i \langle yx_i \rangle. \quad (6)$$

These entropies form a hierarchy $S_{\text{tot}} \geq S_{\text{dir}} \geq S_{\text{true}} \geq 0$. The difference $I_{\text{true}} = S_{\text{tot}} - S_{\text{true}}$ is the true mutual information between the inputs and the output.²⁶ The difference $I_{\text{dir}} = S_{\text{tot}} - S_{\text{dir}}$, which lower-bounds I_{true} , is the mutual information between inputs and output in the direct computation [Eq. (1)]. Finally, due to the maximum entropy form of the minimal model, the KL divergence with the true computation also simplifies to a difference in entropies $D_{\text{KL}}(Q||P) = S_{\text{dir}} - S_{\text{true}}$. Thus, in the limit that the model entropy S_{dir} becomes small, we know that $D_{\text{KL}}(Q||P)$ also becomes small, and the model provides a tight approximation to the true computation. Moreover, in this limit the output becomes a deterministic function of the inputs $P(y=1|\mathbf{x}) = \Theta(b + \sum_i w_i x_i)$, where $\Theta(\cdot)$ is the step function. Together, these observations reveal that if S_{dir} is small, then we have $S_{\text{true}} \sim S_{\text{dir}} \sim 0$, and the neuron itself becomes well-described by an MP neuron or perceptron.^{1,4,31}

Optimal inputs. For a given output neuron, we would like to select the n inputs that produce the most accurate minimal model [Eq. (1)]. As discussed above, the KL divergence between the model and the true computation reduces to a difference in entropies $D_{\text{KL}}(Q||P) = S_{\text{dir}} - S_{\text{true}}$. Thus, the optimal inputs, which give the most accurate predictions for the output, are the ones that produce the maximum entropy model $P(y|\mathbf{x})$ with minimum entropy S_{dir} . This is an instance of the minimax entropy principle, which provides a general strategy for selecting the optimal constraints in maximum entropy models.^{33,34,50}

Greedy algorithm. Searching for the optimal n inputs among the $N - 1$ possibilities is generally infeasible. Instead, we propose a greedy algorithm for growing a locally optimal set of inputs. We begin with the independent model $P(y)$, which has no inputs. We then fit a different model $P(y|x_i)$ for each of the $N - 1$ possible inputs; among these, the optimal input is the one that produces the model with minimum entropy S_{dir} . Repeating this process, we greedily select the optimal input (which minimizes the entropy S_{dir}) at each step until we reach the desired number of inputs n .

Approximate change in entropy. The above algorithm involves fitting $O(nN)$ separate models: one for each of the $O(N)$ possible new inputs during each of the n steps. To improve efficiency, rather than fitting a different model for each possible input, we can approximate the drop in entropy ΔS_{dir} . Using perturbation theory, for a candidate neuron i we expand the change in entropy in the limit of small prediction errors $\langle yx_i \rangle - \langle yx_i \rangle_P$, yielding an analytic approximation for ΔS_{dir} (Supplementary Information). Using this approximation to select the optimal input at each step, the greedy algorithm only requires fitting $O(n)$ models.

Neural data. Our framework can be used to investigate recordings of neuronal activity across different neural systems and species. Since we are interested in understanding the mapping from inputs to output, we focus on large-scale recordings of spatially contiguous populations, where, for each neuron, we may have access to some or most of its inputs. Such recordings are made possible by calcium imaging, wherein animals are genetically modified so that their neurons fluoresce in response to changes in calcium concentration, which in turn follows the electrical activity of the cells. This fluorescence is recorded using an optical microscope with scanning period Δt . Within each period, we binarize activity into active ($x_i = 1$) or silent ($x_i = 0$; Fig. 1a).

We study four recordings of neuronal activity, each measured in previous experiments: One in the mouse hippocampus, two in the mouse visual cortex, and one in the brain of the roundworm *C. elegans*. In the hippocampus, we study $N = 1485$ neurons in the CA1 region as the mouse runs along a virtual track (Fig. 2a); activity is recorded with scanning period $\Delta t = 1/30\text{s}$.¹¹ In the visual cortex, we study $N = 11,445$ neurons recorded with scanning period $\Delta t = 2/3\text{s}$ as the mouse is exposed to two separate visual stimuli: natural images (Fig. 3b) or a grey screen to measure spontaneous activity (Fig. 3c).¹⁰ In *C. elegans*, we study $N = 128$ neurons comprising nearly the entire brain recorded as the animal moves freely with period $\Delta t = 1/1.7\text{s}$ (Fig. 3d).¹² In the hippocampus and *C. elegans*, we investigate the minimal computations for all neurons; while in the visual cortex, we study 100 randomly-selected output neurons.

Due to the sizes of the populations, some neurons never co-fire during the length of each recording, leading to vanishing correlations $\langle yx_i \rangle = 0$. To avoid overfitting and divergences in the model parameters, for each output y , we only consider inputs x_i that co-fired with the output at least once, thus yielding positive correlations $\langle yx_i \rangle > 0$.

Minimal set of inputs. Given an output y and a desired number of inputs n , the greedy algorithm identifies the locally optimal set of inputs $\mathbf{x} = \{x_1, \dots, x_n\}$; however, we still need a principled method for choosing n . At each stage of the greedy algorithm, we have a model $P(y|\mathbf{x})$ with n inputs. We can use this model to predict the correlations $\langle yx_i \rangle_P$ with the other $N - n - 1$ neurons in the population. If all of these predictions are correct—that is, if they match the true correlations $\langle yx_i \rangle$ within experimental errors—then including another input amounts to fitting statistical noise. Thus, for each output neuron, we continue selecting inputs greedily until we reach a number n^* for which the model predicts all other correlations. Specifically, we terminate the greedy algorithm when $|\langle yx_i \rangle - \langle yx_i \rangle_P| \leq 2\sqrt{\langle yx_i \rangle}$ for all neurons i with positive correlations $\langle yx_i \rangle > 0$, where $\sqrt{\langle yx_i \rangle}$ is the standard deviation of yx_i in the data (assuming Poisson statistics). In this way, n^* defines the minimal number of inputs needed for the model to match all of the (positive) direct correlations, either by fitting or prediction. Importantly, we confirm that this avoids overfitting (Supplementary Information).

Higher-order dependencies. The dependencies between inputs and output are encoded in correlations. As discussed above, the direct dependence $P(y|x_i)$ is uniquely defined by the averages $\langle y \rangle$ and $\langle x_i \rangle$ and the correlation $\langle yx_i \rangle$.

The 2nd-order dependence $P(y|x_i, x_j)$ is defined by the direct dependencies $P(y|x_i)$ and $P(y|x_j)$ plus the 2nd-order correlation $\langle yx_i x_j \rangle$. Thus, given a model that matches the direct dependencies, predicting the 2nd-order dependencies amounts to predicting the 2nd-order correlations, as in Fig. 7a. More generally, given a model that matches all of the $(k - 1)^{\text{th}}$ -order dependencies, predicting k^{th} -order dependencies amounts to predicting the corresponding k^{th} -order correlations (Fig. 7c,d).

Error correction. To understand whether the inferred computations exhibit error correction, we artificially remove (or ablate) inputs and study how this impacts the predicted output (Fig. 6f).⁵¹ Given a direct computation $P(y|\mathbf{x})$, we remove an input i by marginalizing over its activity, yielding a new model

$$\tilde{P}(y|\mathbf{x}) = \frac{\sum_{x_i} P(y|\mathbf{x})Q(\mathbf{x})}{\sum_{x_i} Q(\mathbf{x})}, \quad (7)$$

where $Q(\mathbf{x})$ is the empirical distribution over inputs. Note that we do not re-fit the model parameters, we simply marginalize the original model over the ablated inputs. After removing a given fraction of inputs, we compute the mutual information $S_{\text{tot}} - S(\tilde{P})$ between the output and the remaining inputs (Fig. 6g) as well as the prediction error $\frac{1}{L} \sum_{\ell} (1 - \tilde{P}(y(\ell)|\mathbf{x}(\ell)))$ (Fig. 6h). In practice, we marginalize over a specified fraction of the population and repeat the above analysis for each remaining neuron as the output. We then average over all of the output neurons and 100 random realizations of this marginalization process.

Data Availability

The data analyzed in this paper are openly available at
github.com/ChrisWLynn/Minimal_computation.

Code Availability

The code used to perform the analyses in this paper is openly available at
github.com/ChrisWLynn/Minimal_computation.

Supplementary Information. Supplementary text and figures accompany this paper.

Acknowledgements. We thank P. Dixit, B. Machta, D. Clark, T. Geiller, M. Leighton, D. Carcamo, N. Weaver, and Q. Yu for enlightening discussions and comments on earlier versions of the paper. We also acknowledge support from the Department of Physics and the Quantitative Biology Institute at Yale University.

Author Contributions. C.W.L. conceived the project, designed the models, performed the analysis, and wrote the manuscript and Supplementary Information.

Competing Interests. The author declares no competing financial interests.

Corresponding Author. Correspondence and requests for materials should be addressed to C.W.L. (christopher.lynn@yale.edu).

Supplementary Information

1. Introduction

In this Supplementary Information, we provide extended analysis and discussion to support the results in the main text. In Sec. 2, we derive an analytic approximation to the drop in entropy from including an additional input in the minimal computation; we use this approximation to speed up the greedy algorithm for identifying optimal inputs. In Sec. 3, we demonstrate that our procedure for selecting the complete number of inputs n^* avoids overfitting the activity of the output neuron. In Sec. 4, we show that the minimal computation predicts the complex higher-order dependencies between neurons consistently across different species and neural systems. In Sec. 5, we explore the structures of the inferred interactions in different neuronal populations. Finally, in Sec. 6, we demonstrate that the minimal computation achieves exact inference in the Ising model, which has long been used as a simplified model of recurrent neuronal activity.

2. Approximate change in entropy

Consider a binary output $y \in \{0, 1\}$ and n binary inputs $\mathbf{x} = \{x_1, \dots, x_n\} \in \{0, 1\}^n$. The maximum entropy computation consistent with the direct dependencies $P(y|x_j)$, $1 \leq j \leq n$, is given by

$$P(y|\mathbf{x}) = \frac{1}{Z(\mathbf{x})} e^{y(b + \sum_{j=1}^n w_j x_j)}, \quad (8)$$

where $Z(\mathbf{x}) = 1 + e^{b + \sum_{j=1}^n w_j x_j}$ ensures normalization. For ease of derivation, we define $x_0 = 1$ and $w_0 = b$, yielding

$$P(y|\mathbf{x}) = \frac{1}{Z(\mathbf{x})} e^{y \sum_{j=0}^n w_j x_j}. \quad (9)$$

The entropy of the model takes the form

$$S_{\text{dir}} = \langle \log Z(\mathbf{x}) \rangle_{\mathbf{x}} - \sum_{j=0}^n w_j \langle y x_j \rangle, \quad (10)$$

where $\langle \cdot \rangle_{\mathbf{x}}$ represents an empirical average over the inputs \mathbf{x} , and $\langle \cdot \rangle$ represents an empirical average over the inputs and the output y .

We want to derive an analytic approximation to the drop in entropy ΔS_{dir} after including a new input x_i in the model. Using perturbation theory, we can expand ΔS_{dir} in the limit of a small prediction error $\langle yx_i \rangle - \langle yx_i \rangle_P$, where $\langle yx_i \rangle_P = \langle \sum_y yx_i P(y|\mathbf{x}) \rangle_{\mathbf{x}}$ is the correlation predicted by the existing model (without x_i as an input, or, equivalently, with $w_i = 0$). To second order, we have

$$\Delta S_{\text{dir}} = (\langle yx_i \rangle - \langle yx_i \rangle_P) \frac{dS_{\text{dir}}}{d\langle yx_i \rangle_P} \Bigg|_{w_i=0} + \frac{1}{2} (\langle yx_i \rangle - \langle yx_i \rangle_P)^2 \frac{d^2 S_{\text{dir}}}{d\langle yx_i \rangle_P^2} \Bigg|_{w_i=0}. \quad (11)$$

The first derivative takes the form

$$\frac{dS_{\text{dir}}}{d\langle yx_i \rangle_P} = \frac{d\langle \log Z(\mathbf{x}) \rangle_{\mathbf{x}}}{d\langle yx_i \rangle_P} - w_i - \sum_{j=0}^n \left(\langle yx_j \rangle \frac{dw_j}{d\langle yx_i \rangle_P} + w_j \frac{d\langle yx_j \rangle}{d\langle yx_i \rangle_P} \right). \quad (12)$$

From the maximum entropy constraints, we know that $\frac{d\langle yx_j \rangle}{d\langle yx_i \rangle_P} = 0$. We also have

$$\frac{d\langle \log Z(\mathbf{x}) \rangle_{\mathbf{x}}}{d\langle yx_i \rangle_P} = \sum_{j=0}^n \frac{\partial \langle \log Z(\mathbf{x}) \rangle_{\mathbf{x}}}{\partial w_j} \frac{dw_j}{d\langle yx_i \rangle_P} = \sum_{j=0}^n \langle yx_j \rangle_P \frac{dw_j}{d\langle yx_i \rangle_P} = \sum_{j=0}^n \langle yx_j \rangle \frac{dw_j}{d\langle yx_i \rangle_P}. \quad (13)$$

Plugging into Eq. (12), we have $\frac{dS_{\text{dir}}}{d\langle yx_i \rangle_P} = -w_i$. Thus, to first order, ΔS_{dir} vanishes.

The second derivative is given by

$$\frac{d^2 S_{\text{dir}}}{d\langle yx_i \rangle_P^2} = -\frac{dw_i}{d\langle yx_i \rangle_P} = -\left(\frac{d\langle yx_i \rangle_P}{dw_i}\right)^{-1}. \quad (14)$$

We have

$$\frac{d\langle yx_i \rangle_P}{dw_i} = \frac{\partial \langle yx_i \rangle_P}{\partial w_i} + \sum_{j=0}^n \frac{\partial \langle yx_i \rangle_P}{\partial w_j} \frac{dw_j}{dw_i}. \quad (15)$$

We define the matrix

$$M_{ij} = \frac{\partial \langle yx_i \rangle_P}{\partial w_j} \quad (16)$$

$$= \left\langle \frac{\partial}{\partial w_j} \frac{1}{Z(\mathbf{x})} \sum_y yx_i e^{y(w_i x_i + \sum_{j=0}^n w_j x_j)} \right\rangle_{\mathbf{x}} \quad (17)$$

$$= \left\langle \frac{1}{Z(\mathbf{x})} \sum_y y^2 x_i x_j e^{y(w_i x_i + \sum_{j=0}^n w_j x_j)} - \frac{1}{Z(\mathbf{x})^2} \left(\sum_y yx_i e^{y(w_i x_i + \sum_{j=0}^n w_j x_j)} \right) \left(\sum_{y'} y' x_j e^{y'(w_i x_i + \sum_{j=0}^n w_j x_j)} \right) \right\rangle_{\mathbf{x}} \quad (18)$$

$$= \langle yx_i x_j \rangle_P - \langle yy' x_i x_j \rangle_P. \quad (19)$$

The derivative $\frac{dw_j}{dw_i}$ arises from the fact that, as w_i changes, the existing Lagrange multipliers w_j must change to maintain the maximum entropy constraints $\langle yx_j \rangle_P = \langle yx_j \rangle$. Thus, we have

$$0 = \frac{d\langle yx_j \rangle_P}{dw_i} = \frac{\partial \langle yx_j \rangle_P}{\partial w_i} + \sum_{k=0}^n \frac{\partial \langle yx_j \rangle_P}{\partial w_k} \frac{dw_k}{dw_i}. \quad (20)$$

Defining the $(n+1) \times (n+1)$ matrix $\tilde{M}_{jk} = M_{jk}$ for all $j, k = 0, \dots, n$, we can solve for

$$\frac{dw_j}{dw_i} = - \sum_{k=0}^n (\tilde{M}^{-1})_{jk} M_{ki}. \quad (21)$$

Plugging into Eqs. (14-15), we have

$$\frac{d^2 S_{\text{dir}}}{d\langle yx_i \rangle_P^2} = - \left(\frac{d\langle yx_i \rangle_P}{dw_i} \right)^{-1} = - \left(M_{ii} - \sum_{j,k=0}^n M_{ij} (\tilde{M}^{-1})_{jk} M_{ki} \right)^{-1} \quad (22)$$

We therefore arrive at an analytic approximation to the change in entropy

$$\Delta S_{\text{dir}} = - \frac{1}{2} \frac{(\langle yx_i \rangle - \langle yx_i \rangle_P)^2}{M_{ii} - \sum_{j,k=0}^n M_{ij} (\tilde{M}^{-1})_{jk} M_{ki}}. \quad (23)$$

3. Restricting inputs avoids overfitting

When modeling the output of a neuron as a function of inputs using Eq. (8), we need to make sure we are not overfitting the data, thus leading to an artificially low entropy S_{dir} . For a given output neuron, we use a greedy algorithm to iteratively select the n optimal inputs that provide the best description of the output. Each time we add a new input x_i to the model, we include an additional constraint on the direct dependence $P(y|x_i)$, which leads to a lower entropy S_{dir} . In large populations, such as those in the hippocampus and visual cortex studied in the main text, if we include all possible inputs to a given output neuron, then the entropy S_{dir} drops to zero (Fig. 3 in the main text), and we have likely overfit the data.

To avoid overfitting, we terminate the greedy algorithm when the model is able to predict the direct dependencies $P(y|x_i)$ for all neurons x_i that are not included as inputs in the model (within experimental errors). This ensures that we do not constrain any dependencies that the model can already predict, which would amount to fitting statistical noise. Note that we only consider neurons

with positive correlations $\langle yx_i \rangle > 0$, such that the dependencies $P(y|x_i)$ are well-defined. Upon termination of the greedy algorithm, we arrive at a model (which we refer to as “complete”) with n^* inputs that captures the direct dependencies $P(y|x_i)$ on all other neurons in the population (with $\langle yx_i \rangle > 0$), either by fitting or prediction.

Here, we demonstrate that by restricting the number of inputs we avoid overfitting. For each of the four recordings analyzed in the main text, we randomly divide the samples of activity into a training set (90%) and test set (10%). For each neuron, we infer the minimal computations in the training data as we increase the number of optimal inputs n . We then compute the negative log-likelihood of each model in both the training and test data,

$$\ell = -\langle \log P(y|\mathbf{x}) \rangle_{\text{train}} \quad \text{and} \quad \ell_{\text{test}} = -\langle \log P(y|\mathbf{x}) \rangle_{\text{test}}, \quad (24)$$

where $\langle \cdot \rangle_{\text{train}}$ and $\langle \cdot \rangle_{\text{test}}$ represent empirical averages over the training and test data, respectively. For the hippocampus and visual cortex, as we increase the number of inputs n , we see that the ratio ℓ_{test}/ℓ remains small until we reach n^* ; for $n > n^*$, the model begins fitting dependencies $P(y|x_i)$ that it can already predict, and ℓ_{test} increases dramatically relative to ℓ (Fig. S6a-c). For *C. elegans*, we see that the log-likelihood ratio ℓ_{test}/ℓ doesn’t increase until $n \gtrsim 10n^*$, which indicates that one might be able to increase the number of inputs n^* in the complete model without overfitting (Fig. S6d).

We also consider the model errors directly,

$$\varepsilon = \langle 1 - P(y|\mathbf{x}) \rangle_{\text{train}} \quad \text{and} \quad \varepsilon_{\text{test}} = \langle 1 - P(y|\mathbf{x}) \rangle_{\text{test}}. \quad (25)$$

Just as for the log-likelihoods, across all populations, we find that the ratio $\varepsilon_{\text{test}}/\varepsilon$ remains small for $n \leq n^*$ (Fig. S6e-h). In the hippocampus and visual cortex, the test errors increase sharply for $n > n^*$, indicating overfitting (Fig. S6e-g); while in *C. elegans*, the test errors don’t increase significantly until $n \gtrsim 10n^*$ (Fig. S6h). Together, these results demonstrate that, by limiting the number of inputs to n^* , the complete models avoid overfitting the data. In turn, this tells us that the low entropies S_{dir} of the complete models are not due to overfitting (Fig. 3f in the main text); instead, they indicate that the vast majority of neuronal variability is explained by simple compu-

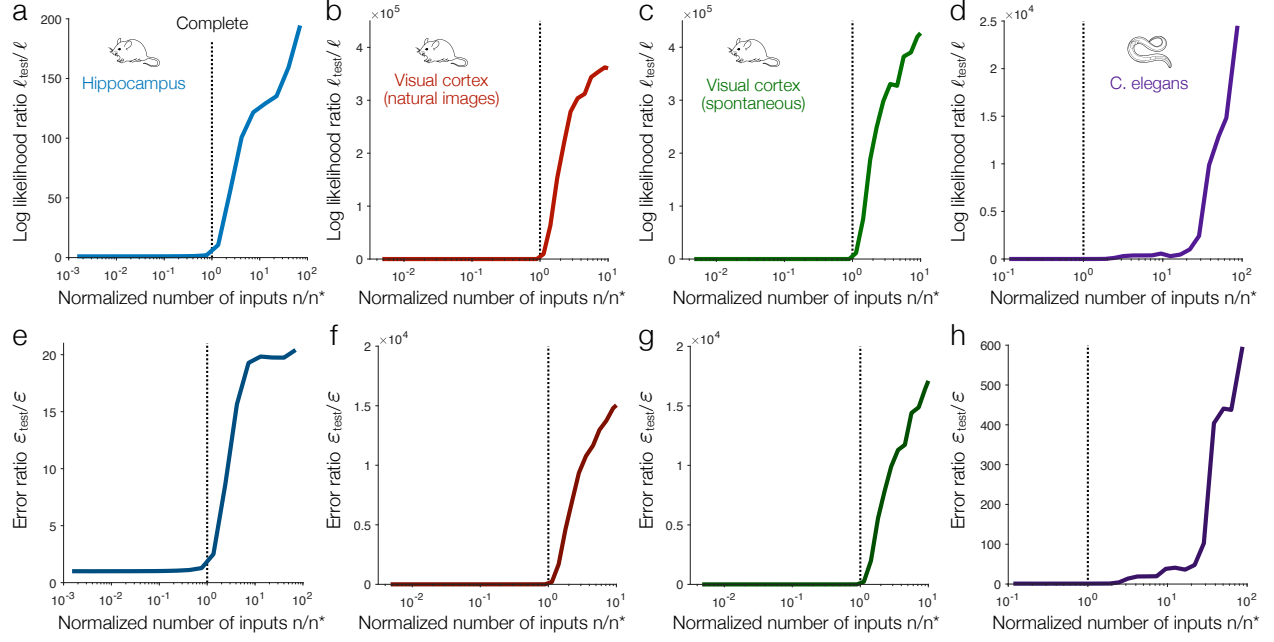


Fig. S6 | Training and test errors. **a-d**, Ratio of test and training log-likelihoods ℓ_{test}/ℓ versus the number of inputs n normalized by n^* for populations of neurons in the mouse hippocampus (**a**),¹¹ mouse visual cortex during responses to natural images (**b**) and spontaneous activity (**c**),¹⁰ and the brain of *C. elegans* (**d**).¹² Dashed lines indicate the complete model with $n = n^*$. **e-h**, Ratio of test and training errors $\varepsilon_{\text{test}}/\varepsilon$ versus the number of inputs n normalized by n^* for the same data as **a-d**. Values in the hippocampus are averaged over all $N = 1485$ neurons in the population (**a** and **e**); values in the visual cortex are averaged over 100 randomly-selected neurons among a population of $N = 11,445$ (**b**, **c**, **f**, and **g**); and values in *C. elegans* are averaged over all $N = 128$ neurons in the population (**d** and **h**).

tations with relatively small numbers of inputs.

4. Predicting higher-order dependencies

Given the direct dependencies $P(y|x_i)$, the minimal computation [Eq. (8)] is maximally random with regard to all complex higher-order dependencies. Thus, if the model is capable of predicting the higher-order dependencies on two, three, or more inputs, then these can be viewed as emerging naturally from simpler direct dependencies. As discussed in the main text, predicting a given k^{th} -order dependence $P(y|x_1, \dots, x_k)$ is equivalent to predicting the correlations between

the output y and all subsets of the k inputs. Thus, if the model captures all of the $k - 1^{\text{th}}$ -order dependencies, all that remains is the k^{th} -order correlation $\langle yx_1 \cdots x_k \rangle$.

As discussed above, for each output neuron y , we use our greedy algorithm to identify the smallest number of inputs n^* for which the model captures all of the positive correlations $\langle yx_i \rangle > 0$ in the population; this defines our complete model. Across each of the populations, we confirm that our complete models match all of the direct correlations within experimental errors (Fig. S7a-d) and, therefore, capture all of the direct dependencies $P(y|x_i)$.

Thus, to predict the second-order dependencies $P(y|x_i, x_j)$, we need only predict the second-order correlations $\langle yx_i x_j \rangle$. In Fig. S7i-l, we show that our models predict nearly all of the second-order correlations within experimental errors. Moreover, the minimal computations correctly predict an even larger proportion of the third-order (Fig. S7i-l) and fourth-order (Fig. S7m-p) correlations. Together, these results demonstrate that our minimal computation is capable of predicting the higher-order dependencies on combinations of two, three, or four inputs. In turn, this indicates that the vast majority of higher-order dependencies are explained simple direct dependencies, rather relying on complex interactions between inputs.

5. Model structures

After constructing the complete model for each output neuron, we have the opportunity to investigate the structures of the inferred computations. In the main text, we showed in the mouse hippocampus that the inferred input weights w_i exhibited four key features. First, the weights are sparse, with only a small number of inputs n^* needed to explain all of a neuron's pairwise dependencies (Fig. 3e in the main text). Second, the distribution of magnitudes is heavy-tailed (specifically log-normal), with some rare weights that are orders of magnitude stronger than average (Fig. S8a). Third, the weights are evenly split between positive and negative, reflecting a delicate balance between excitatory and inhibitory interactions (Fig. S8a). Finally, unlike existing maximum entropy models,^{21,33,35} the weights are highly directed, with the connection strength

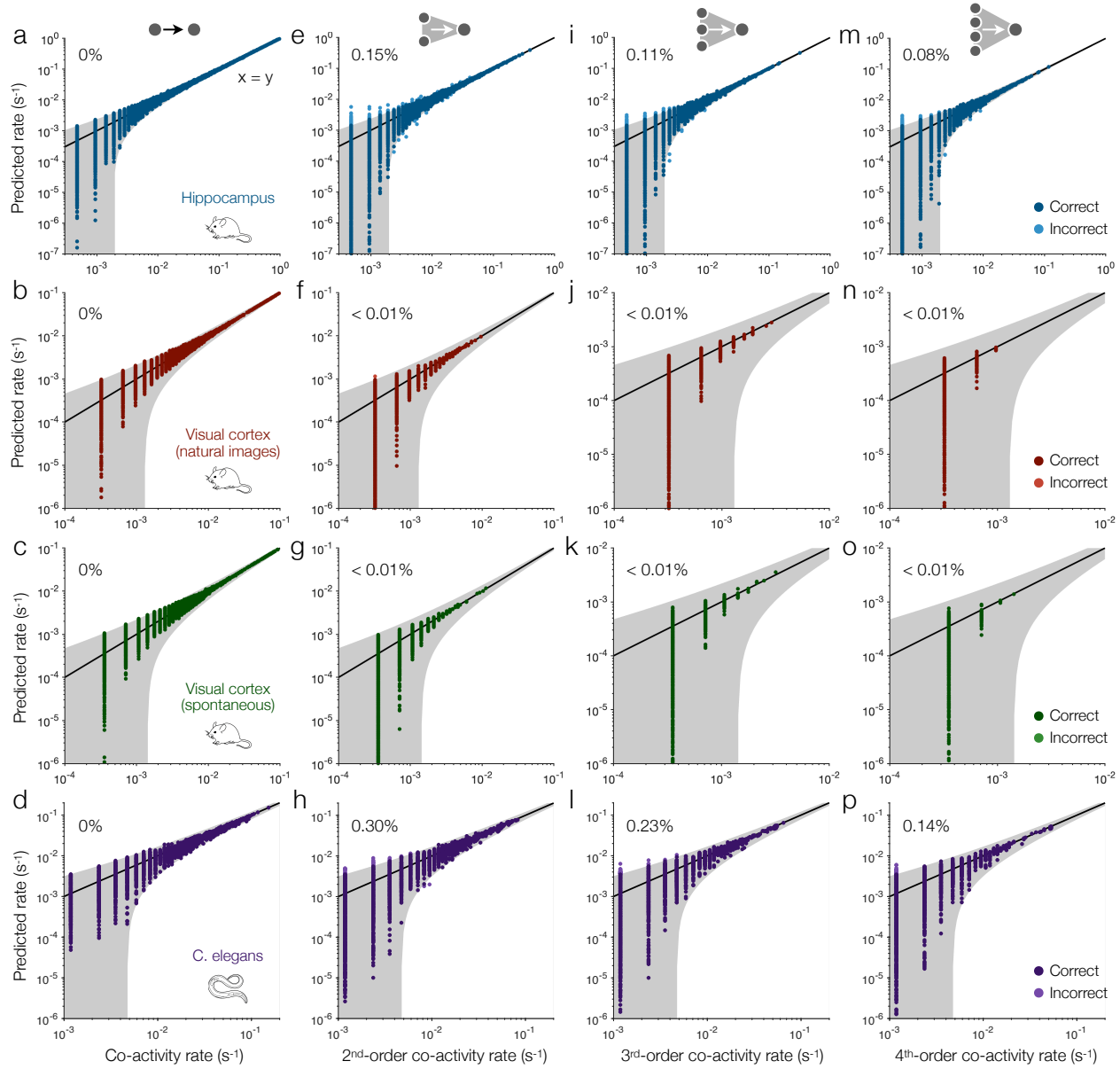


Fig. S7 | Predicting higher-order dependencies. **a-d**, Co-activity rates $\langle yx_i \rangle / \Delta t$ predicted by complete models versus those in the data for populations of neurons in the mouse hippocampus (**a**),¹¹ mouse visual cortex during responses to natural images (**b**) and spontaneous activity (**c**),¹⁰ and the brain of *C. elegans* (**d**).¹² Lines illustrate equality, shaded regions represent two standard deviations of experimental errors, dark points indicate correct predictions (within errors), light points indicate incorrect predictions, and percentages define the proportion of incorrect predictions. By the definition of the complete models, they correctly capture all co-activity rates, either by fitting or prediction. **e-p**, Second-order co-activity rates $\langle yx_i x_j \rangle / \Delta t$ (**e-h**), third-order co-activity rates $\langle yx_i x_j x_k \rangle / \Delta t$ (**i-l**), and fourth-order co-activity rates $\langle yx_i x_j x_k x_\ell \rangle / \Delta t$ (**m-p**) predicted by complete models versus those in the

data for the same populations as **a-d**. For the mouse hippocampus (blue) and *C. elegans* (purple) populations, we consider all $N = 1485$ and $N = 128$ neurons as outputs, respectively. For the mouse visual cortex (red and green), we consider 100 random output neurons within the population of $N = 11,445$ cells. For the direct co-activity rates (**a-d**), for each output neuron y , we consider all positive co-activities in the populations. For the second-order (**e-h**), third-order (**i-l**), and fourth-order (**m-p**) co-activity rates, for each output neuron, we consider 100 randomly-selected positive co-activities in the hippocampal (blue) and *C. elegans* (purple) populations and 10^4 randomly-selected positive co-activities in the visual cortex recordings (red and green).

from input i to output j differing significantly from the reverse. These sparse, heavy-tailed, balanced, and directed weights are universal features of synaptic connectivity observed across brain regions and species.^{14, 15, 39–42}

For recordings in the mouse visual cortex and *C. elegans*, we have already seen that the connectivity sparse (Fig. 3e in the main text), with the complete models requiring an even smaller number of inputs n^* than in the mouse hippocampus. In Fig. S8b-d, we also confirm that the inferred weights w_i are close to log-normally distributed (i.e., heavy-tailed) and quite evenly split between positive and negative (i.e., balanced). Since the weights are also directed, we find that the inferred connectivities share the same four key features across each of the recordings.

In the hippocampal population, we saw in the main text that positive (negative) input weights w_i tend to produce positive (negative) correlations between the inputs and output (Fig. S8e). In Fig. S8f-h, we observe the same relationship in the mouse visual cortex and *C. elegans* recordings. Finally, we consider the mutual information $I_{\text{dir}} = S_{\text{tot}} - S_{\text{dir}}$ between the inputs and output in the minimal computation, which provides a tight upper bound on the true mutual information $I_{\text{true}} = S_{\text{tot}} - S_{\text{true}}$. In the hippocampus, we find that the mutual information increases linearly with the total entropy S_{tot} , with each bit generated by a neuron encoding a consistent 0.87 bits of information about its inputs (Fig. S8i). We confirm similar linear relationships across the mouse visual cortex and *C. elegans* recordings (Fig. S8j-l). Together, these results demonstrate that the nature of inferred computations remains strikingly consistent across species and neural systems.

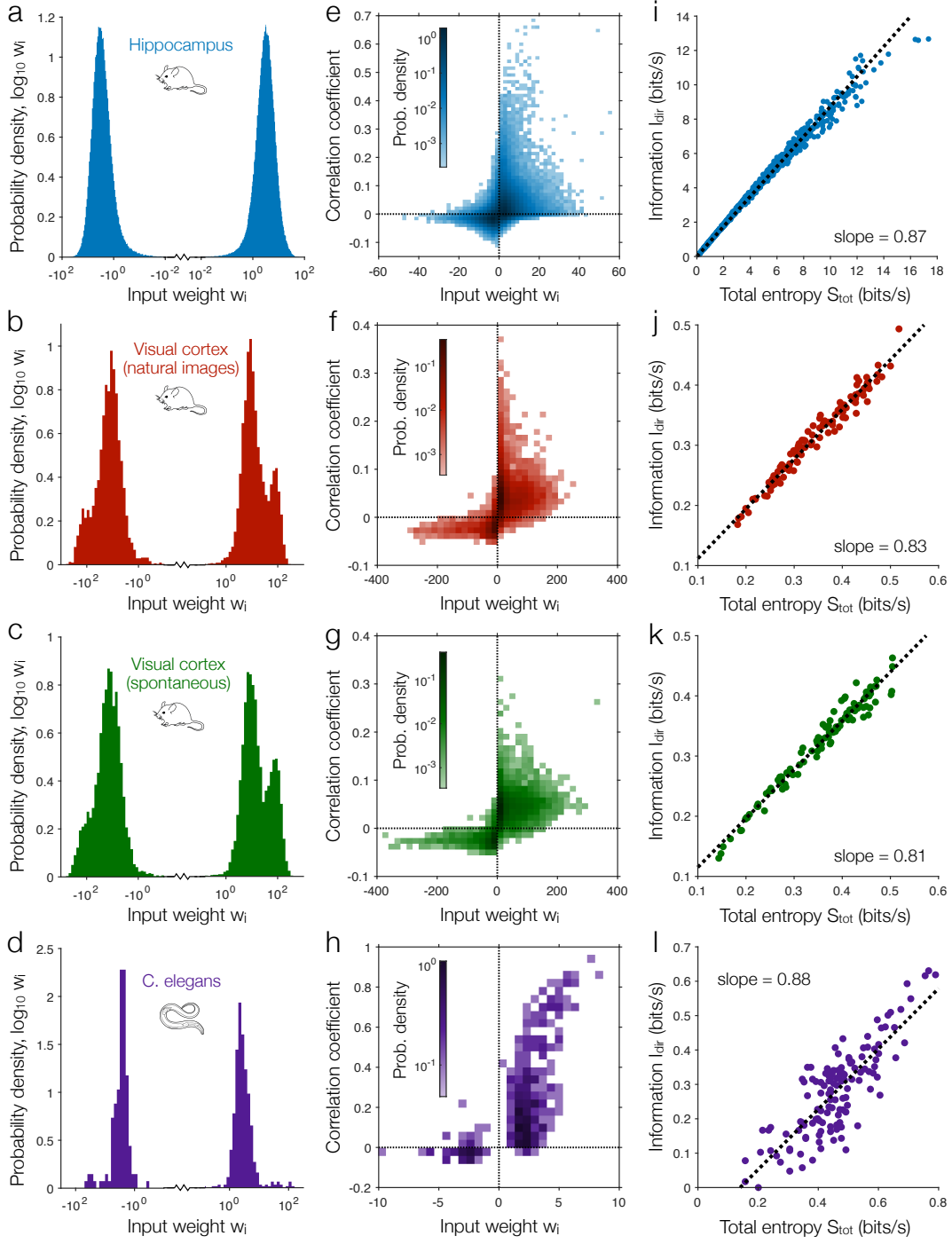


Fig. S8 | Structure of complete models. **a-d**, Distribution of inferred input weights w_i over all complete models in populations in the mouse hippocampus (**a**),¹¹ mouse visual cortex during responses to natural images (**b**) and spontaneous activity (**c**),¹⁰ and the brain of *C. elegans* (**d**).¹² **e-h**, Probability density of the correlation coefficient and corresponding input weight w_i over all input-output pairs in complete models for the same populations as **a-d**. **i-l**, Information I_{dir} in complete models versus total entropy

S_{tot} (normalized by Δt) across all output neurons; dashed line indicates linear fit. For the mouse hippocampus (blue) and *C. elegans* (purple) populations, we consider all $N = 1485$ and $N = 128$ neurons as outputs, respectively. For the mouse visual cortex (red and green), we consider 100 random output neurons within the population of $N = 11,445$ cells.

6. Exact inference in Ising model

We have seen that the minimal computation in Eq. (8) provides a tight approximation to the activity of real neurons. But how does the model perform in an artificial system where the underlying interactions are known? As a salient example, we consider Ising models, which are equivalent to Hopfield networks (with non-zero temperature),² Boltzmann machines,⁴⁴ and maximum entropy models.^{21,33–35} In each of these forms, the Ising model has provided key insights into neural computation, both in the brain and artificial networks. Here, we show that our minimal computation provides exact inference in the Ising model.

Consider a network with N binary neurons defined by the state vector $\mathbf{x} = \{x_1, \dots, x_N\}$. Each neuron has a bias b_i that influences it toward activity or silence, and neurons interact via a symmetric interaction matrix $W_{ij} = W_{ji}$. The joint probability of a given activity state is defined by the Boltzmann distribution

$$P(\mathbf{x}) = \frac{1}{Z} e^{\sum_i b_i x_i + \frac{1}{2} \sum_{ij} W_{ij} x_i x_j}, \quad (26)$$

where

$$Z = \sum_{\mathbf{x} \in \{0,1\}^N} e^{\sum_i b_i x_i + \frac{1}{2} \sum_{ij} W_{ij} x_i x_j} \quad (27)$$

is the partition function, which ensures normalization.

Suppose we want to study the output of one neuron (say x_i) in response to the remaining neurons $\mathbf{x}_{-i} = \{x_1, \dots, x_{i-1}, x_{i+1}, \dots, x_N\}$. Specifically, we would like to compute the conditional probability $P(x_i | \mathbf{x}_{-i}) = P(\mathbf{x}) / P(\mathbf{x}_{-i})$, where

$$P(\mathbf{x}_{-i}) = \sum_{x_i=0,1} P(\mathbf{x}) = \frac{1}{Z} e^{\sum_{j \neq i} b_j x_j + \frac{1}{2} \sum_{jk \neq i} W_{jk} x_i x_j} (1 + e^{b_i + \sum_j W_{ij} x_j}). \quad (28)$$

We therefore have

$$P(x_i|\boldsymbol{x}_{-i}) = \frac{e^{x_i(b_i + \sum_j W_{ij}x_j)}}{1 + e^{b_i + \sum_j W_{ij}x_j}} = \sigma(b_i + \sum_j W_{ij}x_j). \quad (29)$$

This tells us that the conditional probability of one Ising variable in response to the rest of the system takes the precisely the same form as the minimal computation in Eq. (8). Thus, given the direct dependencies $P(x_i|x_j)$ for all $j \neq i$, our minimal model is guaranteed to recover to the correct bias b_i and weights W_{ij} . This approach provides an efficient method for inference in high-dimensional Ising models.⁵²

References

1. McCulloch, W. S. & Pitts, W. A logical calculus of the ideas immanent in nervous activity. *Bull. Math. Biophys.* **5**, 115–133 (1943).
2. Hopfield, J. J. Neural networks and physical systems with emergent collective computational abilities. *Proc. Natl. Acad. Sci. U.S.A.* **79**, 2554–2558 (1982).
3. Rosenblatt, F. *Principles of Neurodynamics: Perceptrons and the Theory of Brain* (Spartan Books, 1962).
4. Hertz, J., Krogh, A. & Palmer, R. G. *Introduction to the Theory of Neural Computation* (Addison–Wesley, Redwood City, 1991).
5. Gidon, A. *et al.* Dendritic action potentials and computation in human layer 2/3 cortical neurons. *Science* **367**, 83–87 (2020).
6. Losonczy, A. & Magee, J. C. Integrative properties of radial oblique dendrites in hippocampal CA1 pyramidal neurons. *Neuron* **50**, 291–307 (2006).
7. Polsky, A., Mel, B. W. & Schiller, J. Computational subunits in thin dendrites of pyramidal cells. *Nat. Neurosci.* **7**, 621–627 (2004).
8. Takahashi, N. *et al.* Locally synchronized synaptic inputs. *Science* **335**, 353–356 (2012).
9. London, M. & Häusser, M. Dendritic computation. *Annu. Rev. Neurosci.* **28**, 503–532 (2005).
10. Stringer, C., Pachitariu, M., Steinmetz, N., Carandini, M. & Harris, K. D. High-dimensional geometry of population responses in visual cortex. *Nature* **571**, 361–365 (2019).
11. Gauthier, J. L. & Tank, D. W. A dedicated population for reward coding in the hippocampus. *Neuron* **99**, 179–193 (2018).
12. Dag, U. *et al.* Dissecting the functional organization of the *C. elegans* serotonergic system at whole-brain scale. *Cell* **186**, 2574–2592 (2023).

13. White, J. G., Southgate, E., Thomson, J. N., Brenner, S. *et al.* The structure of the nervous system of the nematode *Caenorhabditis elegans*. *Philos. Trans. R. Soc. Lond. B Biol. Sci.* **314**, 1–340 (1986).
14. Loomba, S. *et al.* Connectomic comparison of mouse and human cortex. *Science* **377**, eabo0924 (2022).
15. Lin, A. *et al.* Network statistics of the whole-brain connectome of *Drosophila*. *Nature* **634**, 153–165 (2024).
16. Hopfield, J. J. & Tank, D. W. Computing with neural circuits: A model. *Science* **233**, 625–633 (1986).
17. Amit, D. J., Gutfreund, H. & Sompolinsky, H. Spin-glass models of neural networks. *Phys. Rev. A* **32**, 1007 (1985).
18. Demas, J. *et al.* High-speed, cortex-wide volumetric recording of neuroactivity at cellular resolution using light beads microscopy. *Nat. Methods* **18**, 1103–1111 (2021).
19. Urai, A. E., Doiron, B., Leifer, A. M. & Churchland, A. K. Large-scale neural recordings call for new insights to link brain and behavior. *Nat. Neurosci.* **25**, 11–19 (2022).
20. Rieke, F., Warland, D., Van Steveninck, R. d. R. & Bialek, W. *Spikes: Exploring the Neural Code* (MIT Press, 1999).
21. Schneidman, E., Berry II, M. J., Segev, R. & Bialek, W. Weak pairwise correlations imply strongly correlated network states in a neural population. *Nature* **440**, 1007 (2006).
22. Jan, Y.-N. & Jan, L. Y. Branching out: Mechanisms of dendritic arborization. *Nat. Rev. Neurosci.* **11**, 316–328 (2010).
23. Poirazi, P. & Papoutsaki, A. Illuminating dendritic function with computational models. *Nat. Rev. Neurosci.* **21**, 303–321 (2020).

24. Petersen, C. C. Whole-cell recording of neuronal membrane potential during behavior. *Neuron* **95**, 1266–1281 (2017).
25. Jaynes, E. T. Information theory and statistical mechanics. *Phys. Rev.* **106**, 620 (1957).
26. Cover, T. M. & Thomas, J. A. *Elements of information theory* (John Wiley & Sons, 2012).
27. Schneidman, E., Still, S., Berry II, M. J. & Bialek, W. Network information and connected correlations. *Phys. Rev. Lett.* **91**, 238701 (2003).
28. Yarotsky, D. Error bounds for approximations with deep ReLU networks. *Neural Netw.* **94**, 103–114 (2017).
29. Tao, Q. *et al.* Piecewise linear neural networks and deep learning. *Nat. Rev. Methods Primers* **2**, 42 (2022).
30. Strong, S. P., Koberle, R., de Ruyter van Steveninck, R. R. & Bialek, W. Entropy and information in neural spike trains. *Phys. Rev. Lett.* **80**, 197 (1998).
31. Block, H.-D. The perceptron: A model for brain functioning. I. *Rev. Mod. Phys.* **34**, 123 (1962).
32. Muroga, S. *Threshold Logic and Its Applications* (John Wiley & Sons, 1972).
33. Lynn, C. W., Yu, Q., Pang, R., Palmer, S. E. & Bialek, W. Exactly solvable statistical physics models for large neuronal populations. *Preprint: arxiv.org/abs/2310.10860* (2023).
34. Lynn, C. W., Yu, Q., Pang, R., Palmer, S. E. & Bialek, W. Exact minimax entropy models of large-scale neuronal activity. *Preprint: arxiv.org/abs/2310.10860* (2023).
35. Meshulam, L., Gauthier, J. L., Brody, C. D., Tank, D. W. & Bialek, W. Collective behavior of place and non-place neurons in the hippocampal network. *Neuron* **96**, 1178–1191 (2017).
36. Moser, E. I., Kropff, E. & Moser, M.-B. Place cells, grid cells, and the brain’s spatial representation system. *Annu. Rev. Neurosci.* **31**, 69–89 (2008).

37. O'Keefe, J. & Conway, D. H. Hippocampal place units in the freely moving rat: why they fire where they fire. *Exp. Brain Res.* **31**, 573–590 (1978).
38. Hafting, T., Fyhn, M., Molden, S., Moser, M.-B. & Moser, E. I. Microstructure of a spatial map in the entorhinal cortex. *Nature* **436**, 801–806 (2005).
39. Lynn, C. W., Holmes, C. M. & Palmer, S. E. Heavy-tailed neuronal connectivity arises from Hebbian self-organization. *Nat. Phys.* 1–8 (2024).
40. Liu, G. Local structural balance and functional interaction of excitatory and inhibitory synapses in hippocampal dendrites. *Nat. Neurosci.* **7**, 373–379 (2004).
41. Van Vreeswijk, C. & Sompolinsky, H. Chaos in neuronal networks with balanced excitatory and inhibitory activity. *Science* **274**, 1724–1726 (1996).
42. Lynn, C. W. & Bassett, D. S. The physics of brain network structure, function and control. *Nat. Rev. Phys.* **1**, 318 (2019).
43. Steinmetz, N. A. *et al.* Neuropixels 2.0: A miniaturized high-density probe for stable, long-term brain recordings. *Science* **372**, eabf4588 (2021).
44. Ackley, D. H., Hinton, G. E. & Sejnowski, T. J. A learning algorithm for Boltzmann machines. *Cog. Sci.* **9**, 147–169 (1985).
45. Dorkenwald, S. *et al.* Neuronal wiring diagram of an adult brain. *Nature* **634**, 124–138 (2024).
46. Shapson-Coe, A. *et al.* A petavoxel fragment of human cerebral cortex reconstructed at nanoscale resolution. *Science* **384**, eadk4858 (2024).
47. Nelder, J. A. & Wedderburn, R. W. Generalized linear models. *J. R. Stat. Soc. Ser. A* **135**, 370–384 (1972).
48. Weber, A. I. & Pillow, J. W. Capturing the dynamical repertoire of single neurons with generalized linear models. *Neural Comput.* **29**, 3260–3289 (2017).

49. Nguyen, H. C., Zecchina, R. & Berg, J. Inverse statistical problems: from the inverse Ising problem to data science. *Adv. Phys.* **66**, 197–261 (2017).
50. Carcamo, D. P. & Lynn, C. W. Statistical physics of large-scale neural activity with loops. *Preprint: arxiv.org/abs/2412.18115* (2024).
51. Meyes, R., Lu, M., de Puiseau, C. W. & Meisen, T. Ablation studies in artificial neural networks. *Preprint: arxiv.org/ab/1901.08644* (2019).
52. Ravikumar, P., Wainwright, M. J. & Lafferty, J. D. High-dimensional Ising model selection using ℓ_1 -regularized logistic regression. *Ann. Statist.* (2010).